PNAS RESEARCH ARTICLE | PLANT BIOLOGY OPEN ACCESS

NKS1/ELMO4 is an integral protein of a pectin synthesis protein complex and maintains Golgi morphology and cell adhesion in *Arabidopsis*

Rahul S. Lathe[a,b,c,1], Heather E. McFarlane[d,e,1,2], Christopher Kesten[a], Liu Wang[a,e], Ghazanfar Abbas Khan[e,f], Berit Ebert[e,g], Eduardo Antonio Ramírez-Rodríguez[d], Shuai Zheng[a], Niels Noord[c], Kristian Frandsen[a], Rishikesh P. Bhalerao[c], and Staffan Persson[a,b,e,h,2]

Edited by Natasha Raikhel, University of California Riverside Center for Plant Cell Biology, Riverside, CA; received January 3, 2024; accepted March 7, 2024

Adjacent plant cells are connected by specialized cell wall regions, called middle lamellae, which influence critical agricultural characteristics, including fruit ripening and organ abscission. Middle lamellae are enriched in pectin polysaccharides, specifically homogalacturonan (HG). Here, we identify a plant-specific *Arabidopsis* DUF1068 protein, called NKS1/ELMO4, that is required for middle lamellae integrity and cell adhesion. NKS1 localizes to the Golgi apparatus and loss of NKS1 results in changes to Golgi structure and function. The *nks1* mutants also display HG deficient phenotypes, including reduced seedling growth, changes to cell wall composition, and tissue integrity defects. These phenotypes are comparable to *qua1* and *qua2* mutants, which are defective in HG biosynthesis. Notably, genetic interactions indicate that NKS1 and the QUAs work in a common pathway. Protein interaction analyses and modeling corroborate that they work together in a stable protein complex with other pectin-related proteins. We propose that NKS1 is an integral part of a large pectin synthesis protein complex and that proper function of this complex is important to support Golgi structure and function.

Arabidopsis | cell walls | cell biology | pectin | Golgi apparatus

Significance

Cell walls are essential to cell morphogenesis, to protect plants against environmental stress, and for an array of products in our daily life. Understanding how plants produce cell wall polymers is therefore important. In this study, we outline how a family of unknown proteins function as a scaffold for key synthesis components of pectin, a central cell wall polymer. Our results thus define a robust pectin synthesis protein complex that is essential for the structure and function of Golgi and for plant tissue integrity. These results add critical information regarding pectin synthesis and cell wall metabolons.

Growing plant cells are surrounded by a primary cell wall: a strong yet flexible extracellular matrix that is largely made of polysaccharides. Cell walls have the strength to resist turgor pressure and to direct cell morphology, but they are flexible enough to allow plant cells to expand. Cellulose microfibrils are the main load-bearing components of primary cell walls and are embedded in a hydrated matrix of pectins and hemicelluloses, with some proteins (1). Pectins are a heterogeneous class of acidic polysaccharides, including homogalacturonan (HG), rhamnogalaturonan (RG) I and RGII (2, 3). Pectins are particularly abundant in the primary cell walls of dicots, such as the model plant, *Arabidopsis thaliana*.

Pectins are made in the Golgi apparatus by the coordinated action of transporters and enzymes. Sugar interconversion enzymes, which are generally cytosolic, generate the nucleotide sugar building blocks for pectin synthesis (4); nucleotide sugar transporters facilitate their movement across Golgi membranes (5); glycosyltransferases (GTs) catalyze their incorporation into pectic polysaccharides (6); and methyltransferases and acetyltransferases further modify some pectins (7). In particular, HG is secreted in a highly methylesterified form (8). Once in the cell wall, HG may be modified by de-esterification, which can affect pectin cross-linking via Ca^{2+}, and ultimately influence the mechanical properties of the cell wall (9, 10). Indeed, a feedback loop exists between mechanical forces and pectin synthesis (11), and pectins are implicated in plant cell morphogenesis (10, 12, 13). For example, during growth symmetry breaking in the *Arabidopsis* hypocotyl, changes to pectin structure precede other changes in the cell cortex and cell wall, including cortical microtubule reorientation and realignment of cellulose deposition (10).

Adjacent plant cells are connected by specialized regions of the cell wall, called middle lamellae. Regulation and degradation of middle lamellae underly critical agricultural characteristics, including fruit ripening (14) and organ abscission (15, 16), such as seed pod shattering (17). Middle lamellae are pectin-rich and particularly enriched in HG (18). Therefore, defects in HG synthesis can lead to loss of cell–cell adhesion and epidermal tissue integrity, with dramatic consequences for plant growth and development (6, 7). Such defects are evident in mutants that affect a member of the GT8 family of putative galacturonosyl transferases (GalATs) called QUASIMODO (QUA)1; *qua1* mutants have reduced levels of HG and displayed decreased growth and epidermal cell separation (6). Similar phenotypes are observed in plants with mutations that affected a pectin methyltransferase, QUA2 (7, 19) and ELMO1 [At2g32580; (20)]. Both the *qua2* and *elmo1* mutants have reduced HG content in their cell walls (21). However, despite the methyltransferase function of QUA2, *qua2* mutants do not display any changes to pectin

Author contributions: R.S.L., H.E.M., R.P.B., and S.P. designed research; R.S.L., H.E.M., C.K., L.W., G.A.K., B.E., E.A.R.-R., S.Z., and N.N. performed research; R.S.L., H.E.M., C.K., L.W., G.A.K., B.E., E.A.R.-R., S.Z., N.N., K.F., and S.P. analyzed data; and R.S.L., H.E.M., C.K., R.P.B., and S.P. wrote the paper.

The authors declare no competing interest.

This article is a PNAS Direct Submission.

[1]R.S.L. and H.E.M. contributed equally to this work.

[2]To whom correspondence may be addressed. Email: h.mcfarlane@utoronto.ca or staffan.persson@plen.ku.dk.

This article contains supporting information online at https://www.pnas.org/lookup/suppl/doi:10.1073/pnas.2321759121/-/DCSupplemental.

Published April 5, 2024.

methylesterification status (19), implying that the HG that is synthesized in *qua2* mutants is efficiently methylesterified by other methyltransferases and that HG synthesis and methylesterification are tightly coupled.

While pectin synthesis occurs in the Golgi apparatus, there is contradictory data as to whether proteins required for HG synthesis are distributed across different Golgi cisterna (8, 22), whether HG synthesis proteins are part of multiprotein complexes (3, 23, 24), or a combination of both models (25, 26). A better understanding of the pectin synthesis machinery and its interactors is required to appreciate the synthesis of this class of polysaccharides and to open the potential for pectin engineering for agricultural improvements. Here, we report that a plant-specific Golgi-localized protein of unknown function (DUF1068)/Na^+ AND K^+-SENSITIVE 1 (NKS1)/ELMO4 interacts with QUA1, QUA2 and GALACTURONOSYLTRANSFERASE 9 (GAUT9) to support HG synthesis, Golgi integrity and cell adhesion. We propose that NKS1 is part of a HG synthesis complex and that this complex is important to support Golgi structure and function.

Results

A DUF1068 Protein, Referred to as NKS1, Is Required for Cell Elongation. Coexpression is a powerful approach to identify functionally related genes (27). Using ATTED-II (28), we identified several genes from the *Arabidopsis* DUF1068 family as co-expressed with primary wall *CELLULOSE SYNTHASE* (*CESA*) genes and pectin biosynthesis-related genes, including GalATs *GAUT9* and *QUA1,* the HG methyltransferase *QUA3*, and many S-adenosylmethionine family transporter genes, which might play important roles in HG-methyltransferase activity (29) (Datasets S1 and S2). We examined T-DNA lines that were annotated to target DUF1068 genes from the coexpression list above. Of the ones we tested, two independent T-DNA lines targeting the DUF1068 gene *At4g30996* [*NKS1*/*ELMO4*; (20, 30)] displayed significant reduction in mean hypocotyl length of 6-d-old etiolated seedlings, compared to wild type (Fig. 1). Moreover, growth kinematics of etiolated seedlings were dramatically affected in the *nks1* mutant hypocotyls compared to wild type (Fig. 1*D*). We refer to these two T-DNA lines as *nks1-2* (SALK_151073) and *nks1-3* (GK-228H05) as *nks1-1* is another T-DNA line used in ref. 30 (*SI Appendix*, Fig. S1*A*). While RT-PCR analysis indicated that the two lines were transcriptional null lines (*SI Appendix*, Fig. S1*B*), qPCR analyses revealed some residual *NKS1* expression in *nks1-2* (Fig. 1*A*). Nevertheless, there was a substantial reduction in *NKS1* expression in the two T-DNA lines and the growth phenotypes of *nks1-2* and *nks1-3* seedlings could be rescued by molecular complementation using fluorescent protein fusions to NKS1, either NKS1–GFP or GFP–NKS1 (Fig. 1*E*). Although NKS1 is ubiquitously expressed (*SI Appendix*, Fig. S1*C*), we primarily observed phenotypes in young seedlings.

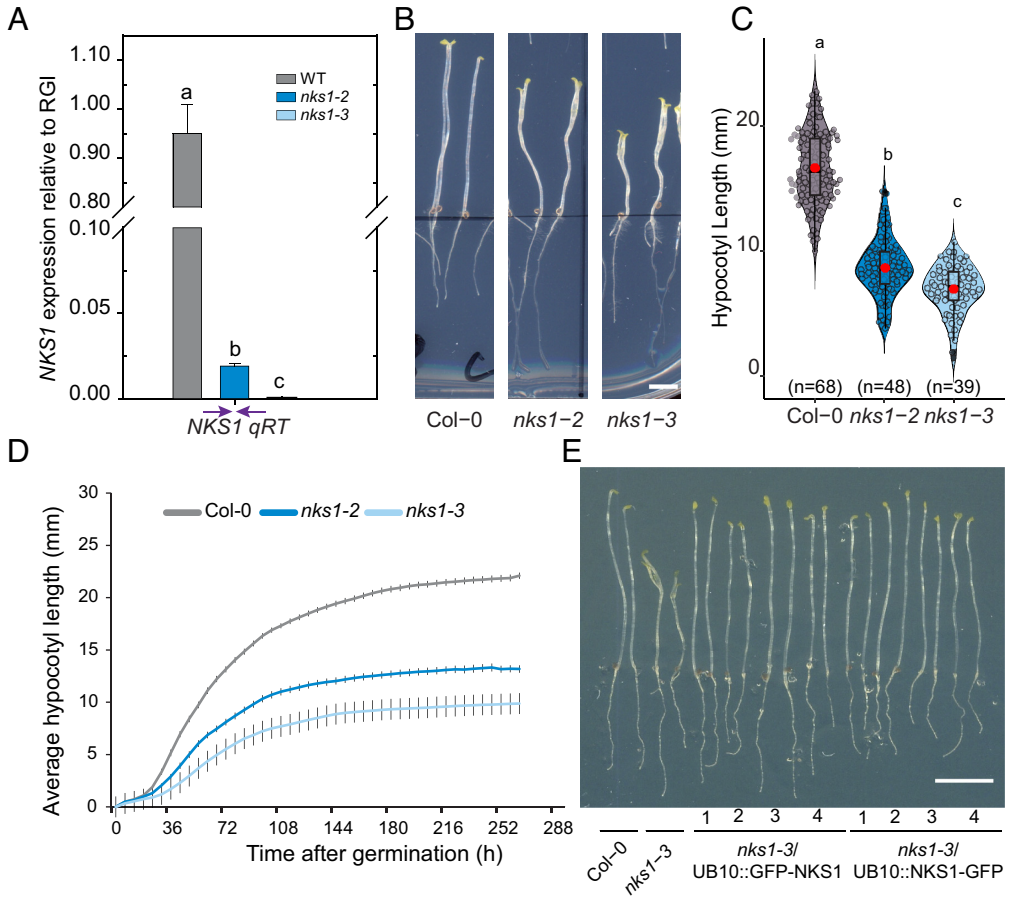

Fig. 1. *nks1* mutants are defective in cell elongation. (*A*) qRT-PCR of *NKS1* transcript levels normalized to reference gene index (RGI) from Col-0, *nks1-2,* and *nks1-3*; bars represent means of three biological replicates ±SD. (*B*) Representative images of 6-d-old etiolated seedlings of Col-0, *nks1-2,* and *nks1-3*. (*C*) Quantification of hypocotyl lengths from 6-d-old etiolated seedlings of Col-0, *nks1-2,* and *nks1-3*; data distribution is outlined by the shape, plot box limits indicate 25th and 75th percentiles, whiskers extend to 1.5 times the interquartile range, median is indicated by a horizontal line, mean by a red dot, individual data points are shown, and n (seedlings) is indicated in parentheses. (*D*) Etiolated hypocotyl growth kinematics of Col-0, *nks1-2,* and *nks1-3* seedlings (n = 15 seedlings); points indicate mean ± SD). (*E*) Representative images of pUB10-GFP-NKS1 and pUB10-NKS1-GFP expressed in the *nks1-3* background along with controls (Col-0 and *nks1-3*); four independent transformation lines are shown for each construct and two seedlings are shown for each genotype. Letters in (*A*) and (*C*) specify statistically significant differences among samples as determined by one way ANOVA followed by Tukey's HSD test ($P < 0.05$). [Scale bars, 2 mm in (*B*) and 5 mm in (*E*).]

Functional Fluorescently Tagged NKS1 Fusions Localize to the Golgi Apparatus. To better understand NKS1 function, we undertook subcellular localization studies of the functional NKS1–GFP and GFP–NKS1 fusion proteins (Fig. 1*E*). Both NKS1–GFP and GFP–NKS1 were localized to doughnut-shaped particles that were rapidly streaming in the cytoplasm of hypocotyl epidermal cells (Fig. 2*A*), which is typical of Golgi-localized proteins. We also generated an NKS1–mRFP fusion for colocalization purposes that displayed similar localization to both GFP fusions. Quantitative colocalization with markers for the ER [HDEL; (31)], the Golgi apparatus [WAVE18/Got1P homolog and WAVE22/SYP32; (32)], the *trans*-Golgi Network [TGN; VHAa1; (33)], and late endosomes [WAVE2/RabF2b and WAVE7/RabF2a; (32)] revealed that NKS1–GFP colocalized with Golgi markers and displayed some overlap with TGN markers (Fig. 2*B* and *SI Appendix*, Fig. S2*A*). To distinguish between the Golgi and TGN, we treated seedlings with Brefeldin A (BFA) for 60 min, which in *Arabidopsis* root cells causes aggregation of TGN and other compartments into BFA bodies, while intact Golgi stacks surround the core of the BFA body (34–36). After BFA treatment, NKS1–GFP localized to discrete puncta around the core of the BFA body, and NKS1–GFP remained highly colocalized with the Golgi marker [XYLT; (37)] but was no longer colocalized with the TGN marker, VHAa1, which was in the core of the BFA bodies (33) (*SI Appendix*, Fig. S2*B*). These data are consistent with those of subcellular proteomics studies, which have detected NKS1 in Golgi fractions (22, 38, 39).

Different Golgi cisternae are associated with different biochemical functions, i.e., the assembly or modification of certain cell wall components (25, 26). To investigate whether NKS1 is associated with certain cisternae, we next crossed the NKS1–GFP or

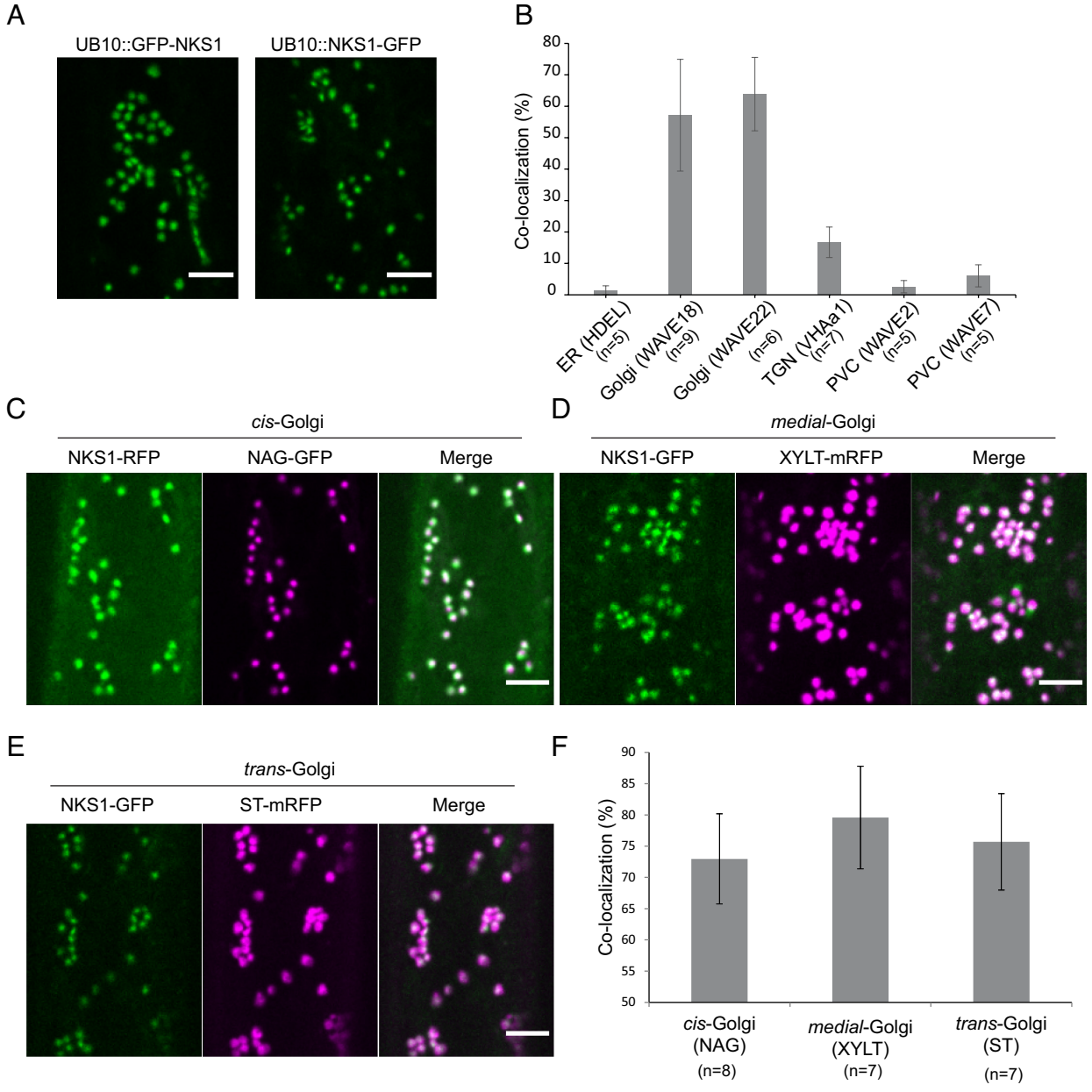

Fig. 2. Functional NKS1–GFP fusion is localized to the Golgi apparatus. (*A*) Representative images NKS1 localization to endomembrane compartments; N- and C-terminal GFP fusion construct localization in single focal plane images of hypocotyl epidermal cells of 3-d-old etiolated seedlings. (*B*) Quantification of colocalization between NKS1 and various endomembrane compartment-specific markers. (*C*–*E*) Representative images of colocalization between NKS1–GFP or NKS1–RFP and Golgi cisternae markers: NAG–GFP (*cis*-Golgi), XYLT-mRFP (*medial*-Golgi), and sialyltransferase (ST)-mRFP (*trans*-Golgi) in hypocotyl epidermal cells of 3-d-old etiolated seedlings. (*F*) Quantification of colocalization percentage between NKS1 and Golgi-cisternae specific markers. In bar charts, bars represent mean ± SD, n (cells, one cell imaged per seedling) is indicated in parentheses. [Scale bars, 5 μm in (*A* and *C*–*E*).]

NKS1–mRFP fluorescent lines with markers for the *cis*-Golgi [NAG; (35)], *medial*-Golgi [XYLT; (37)], or *trans*-Golgi [ST; (40)] to generate dual-labeled fluorescent lines. While NKS1 colocalized with all three markers, the highest degree of colocalization was observed with *medial*-Golgi markers (Fig. 2 *C*–*F*). Together, these results confirm that the functional NKS1–GFP fusion is preferentially localized to *medial*-cisternae of the Golgi apparatus.

NKS1 Is a Plant-Specific Transmembrane Protein with Its DUF1068 Domain Inside the Golgi Lumen. *NKS1* encodes a plant-specific protein of 172 amino acids with a predicted molecular mass of 19 KDa. Genes encoding DUF1068-containing proteins are found throughout land plants (Embryophyta), including *Marchantia polymorpha* and *Physcomitrium patens*, suggesting that DUF1068 function was acquired as plants colonized land (*SI Appendix*, Fig. S3*A*). NKS1 (ELMO4) is part of the ELMO protein family and is distantly related to the recently characterized ELMO1 [(21); *SI Appendix*, Fig. S3*A*]. NKS1 is predicted to contain one transmembrane domain [TM; TmHMM server; (41)] (*SI Appendix*, Fig. S3*B*). This prediction also suggested that the first 17 amino acids in the N terminus of NKS1 are cytoplasmic, which would imply that the amino acids after the TM domain would face the Golgi lumen. To test this prediction, we used a GO-PROMPTO assay (42). Here, we fused the N-terminal part of VENUS (Vn; the first 155 amino acids), or the C-terminal part of VENUS (Vc; the last 84 amino acids), in frame either before (cytosolic reporter) or after (Golgi luminal reporter) the first 52 amino acids of the rat sialyltransferase (ST) protein, which consists of a transmembrane domain targeted to the Golgi apparatus (42). We observed clear fluorescence complementation only when coexpressing Vc-NKS1 with the cytosolic reporter, but not with the luminal reporter (*SI Appendix*, Fig. S3*C*). These results corroborate that the N terminus of NKS1 faces the cytoplasm, while the bulk of the protein, including the DUF1068 domain, is in the Golgi lumen (*SI Appendix*, Fig. S3*D*).

***nks1* Mutants Are Defective in Golgi Structure and Function.** The Golgi localization of NKS1 prompted us to examine the structure and function of the Golgi apparatus in *nks1* mutants. We therefore generated double Golgi marker lines that carried both the *cis*-Golgi marker NAG-EGFP (35) and the *trans*-Golgi marker ST-mRFP (40). Simultaneous, dual color live-cell imaging and object-based colocalization between the two markers demonstrated that these two Golgi markers were significantly further apart in *nks1-3* mutants, relative to wild type (Fig. 3 *A*–*C*). This increased separation between *cis*-Golgi and *trans*-Golgi in *nks1* mutants was not an artifact of faster Golgi stack movement within cells; in fact, measurements of Golgi marker dynamics indicated that Golgi stacks moved significantly slower in *nks1-3* mutants, relative to wild type (Fig. 3*D* and Movies S1 and S2). We therefore examined Golgi structure at high resolution using transmission electron microscopy (TEM) of high-pressure frozen, freeze-substituted hypocotyls and found that Golgi morphology was dramatically affected in *nks1* mutants (Fig. 3*E*). We frequently observed curved Golgi stacks in both alleles of *nks1*, and the proportion of curved Golgi stacks was significantly higher in *nks1* mutants than wild type (Fig. 3*F*). Loss of NKS1 resulted in fewer cisternae per Golgi stack (*SI Appendix*, Table S1), suggesting that the relative distribution of the fluorescent markers may also be shifted in *nks1* Golgi stacks. No other changes to Golgi morphometrics (cisternal length:width, proportion of Golgi stacks with an associated TGN, etc.) were observed (*SI Appendix*, Table S1). Dual-axis transmission electron tomograms of wild type and *nks1-3* Golgi stacks confirmed that Golgi curving was not an artifact of the plane of section and provided additional insight into the Golgi structure defects observed in *nks1* mutants (Fig. 3*G* and Movies S3–S6).

To determine whether the structural changes to the Golgi apparatus affected Golgi function in *nks1* mutants, we assayed a ratiometric marker of soluble protein secretion, sec-GFP (43). Sec-GFP is GFP fused to a signal peptide, which directs the protein to the secretory pathway and ultimately to the apoplast, where the GFP fluorescence is quenched by the low pH; because of the stochastic expression of 35S-driven sec-GFP, especially in epidermal cells, an endomembrane-targeted RFP is produced in equal amounts to sec-GFP; therefore, the ratio of GFP:RFP can be compared across different plants (43). The ratio of GFP:RFP was significantly higher in *nks1-3* mutants compared to wild type (Fig. 3*H* and *SI Appendix*, Fig. S4*A*), indicating a secretion defect. This was not due to any changes in the ratiometric sec-GFP or RFP protein levels in the *nks1-3* mutant compared to wild type (*SI Appendix*, Fig. S4*B*). However, we note that we cannot rule out changes in the RFP reference fluorescence levels due to potential trafficking defects in the *nks1* mutant.

Since secretion flows through both the Golgi apparatus and the TGN, we tested whether TGN structure or function was affected in *nks1* mutants. Using simultaneous dual color live cell imaging and object-based colocalization, we found no significant difference in the distance between a Golgi marker [WAVE18, (32)] and TGN marker [VHAa1, (33)] between wild type and *nsk1-3* (Fig. 3*C* and *SI Appendix*, Fig. S5*A*). There were also no substantial differences in Golgi-TGN association or TGN morphology at the TEM level (*SI Appendix*, Fig. S5*B* and Table S1). To examine anterograde trafficking from the TGN, we tracked the localization of PIN2–GFP (44) after BFA treatment and washout. Since BFA-treatment of *Arabidopsis* root epidermal cells induces aggregation of TGN and endosomes in the BFA body, but leaves Golgi stacks intact and clustered around the BFA body (34–36), signal recovery after BFA washout primarily involves protein secretion from the BFA body/TGN to the plasma membrane. We found no significant differences between the ratio of PIN2–GFP plasma membrane signal compared to intracellular signal or in the number of BFA bodies between wild type and *nks1-3* mutants at any stage of BFA treatment or washout (*SI Appendix*, Fig. S5*C*). Finally, since the plant TGN also functions as an early endosome (45), we assayed endocytosis by tracking uptake of the fluorescent endocytic marker, FM4-64 (46). There were no significant differences in FM4-64 uptake between wild type and *nks1-3* (*SI Appendix*, Fig. S5*D*). Together, these results indicate that while TGN structure and function seem unaffected by loss of NKS1, Golgi apparatus structure and function are impaired in *nks1* mutants.

***nks1* Mutants Are Defective in Cell Adhesion and Cell Wall Pectins.** In addition to the defects in cell elongation, *nks1* mutant seedlings displayed defects in cell adhesion: in cryo-scanning electron microscopy (cryo-SEM), hypocotyl cells of *nks1* mutants seemed to be peeling apart in both epidermal and cortical cell layers (Fig. 4 *A* and *B*). Consistent with a loss of tissue integrity, *nks1* mutant hypocotyls were permeable to toluidine blue dye (*SI Appendix*, Fig. S6*A*).

The cell walls of adjacent plant cells are joined by the middle lamella, a pectin-rich region that is particularly enriched in HG (18); changes in cell wall HG can therefore lead to cell–cell adhesion defects and loss of epidermal tissue integrity (6, 7). HG and other pectins are characterized by high levels of galacturonic acid (GalA) (24). Therefore, we quantified total cell wall monosaccharides by HPAEC-PAD. These experiments revealed a significant reduction in GalA content in *nks1-3* compared to wild type, which was accompanied by a significant increase in arabinose

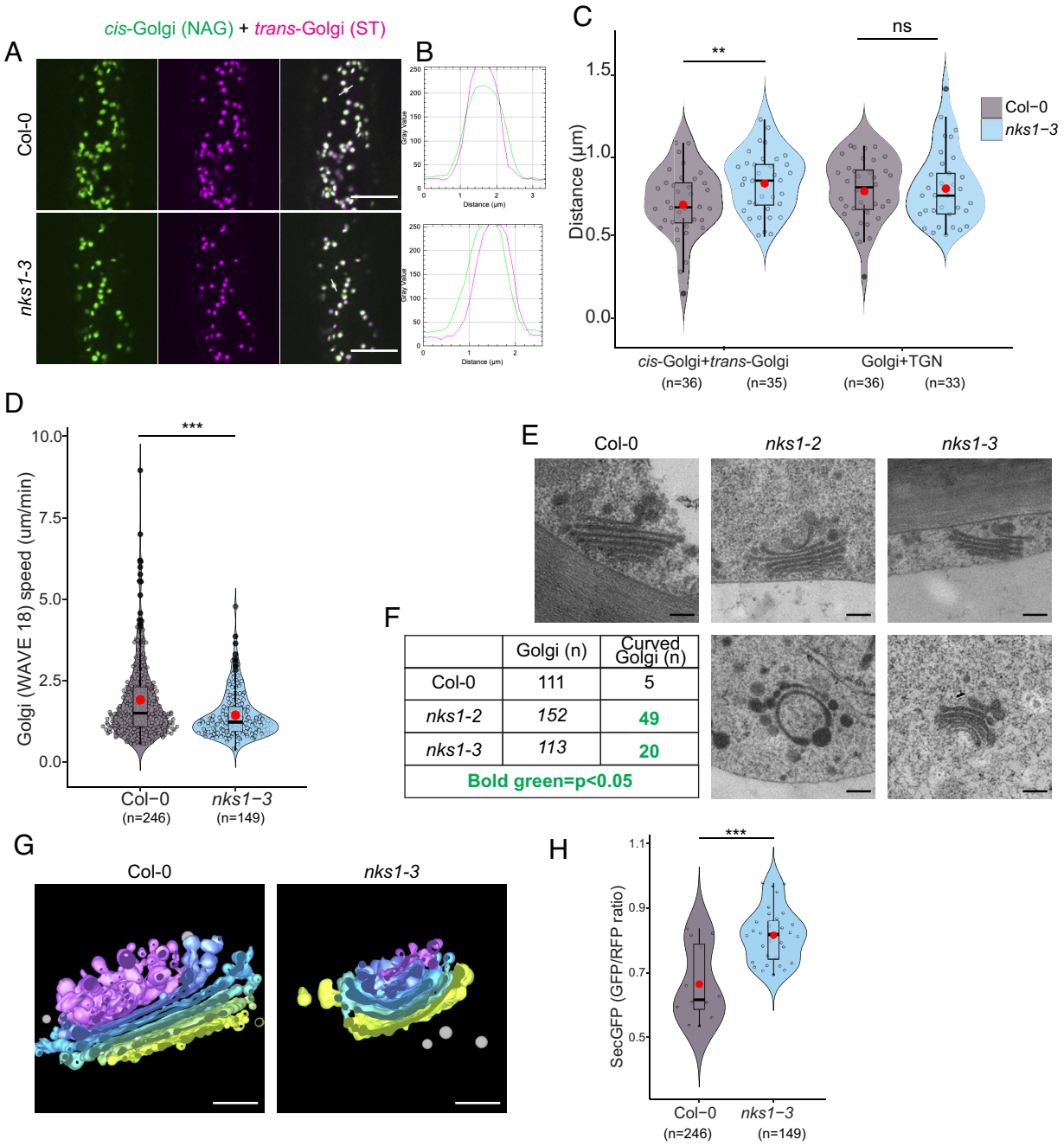

Fig. 3. *nsk1* mutants are defective in Golgi apparatus structure and function. (*A*) Representative images of simultaneous dual-wavelength localization of *cis*-Golgi (NAG) and *trans*-Golgi (ST) dual markers in Col-0 and *nks1-3* hypocotyl epidermal cells of 3-d-old etiolated seedlings. (*B*) Linescan graph showing distance between *cis*-Golgi (NAG) and *trans*-Golgi (ST) dual markers in Col-0 and *nks1-3* from single Golgi particle shown in *A*. (*C*) Quantification of the distance between *cis*-Golgi (NAG) and *trans*-Golgi (ST) dual markers or *medial*-Golgi (WAVE18) and TGN (VHAa1) dual markers in Col-0 and *nks1-3* hypocotyl epidermal cells of 3-d-old etiolated seedlings. (*D*) Quantification of Golgi (WAVE 18) speed in Col-0 and *nks1-3* cells. (*E*) Representative transmission electron microscopy images of Golgi ultrastructure from Col-0, *nks1-2,* and *nks1-3* hypocotyl epidermal cells of 3-d-old etiolated seedlings. (*F*) Quantification of the frequency of Golgi curving in Col-0 and *nks1* alleles. Statistically significant numbers are shown in bold green color ($P < 0.05$, χ^2 test, 1 d.f.). (*G*) Representative electron tomogram models of Col-0 and *nks1-3* Golgi apparatus; the *cis*-most cisterna is labeled in yellow, the *trans*-most cisterna in purple, and cisternae between are labeled by a gradient of green through blue, the TGN is labeled in pink and free vesicles in gray. (*H*) Quantification of SecGFP secretion ratio in Col-0 and *nks1-3* hypocotyl epidermal cells of 3-d-old etiolated seedlings. Asterisks in (*C*, *D*, and *H*) indicate statistically significant difference between Col-0 and *nks1* as determined by unequal variance, two-tailed Student's *t* test, where ***$P < 0.0005$, **$P < 0.005$. In violin plots, data distribution is outlined by the shape, plot box limits indicate 25th and 75th percentiles, whiskers extend to 1.5 times the interquartile range, median is indicated by a horizontal line, mean by a red dot and individual data points are shown, and n is indicated in parentheses. [Scale bars, 10 µm in (*A*), and 200 nm in (*E* and *G*).]

content compared to wild type (Fig. 4*C* and *SI Appendix*, Table S2). Sequential extraction of cell wall polymers confirmed that a significant decrease in GalA in both *nks1* alleles was associated with the CDTA-extracted fraction that mainly extracts calcium cross-linked pectins from the cell wall. *nks1* mutants also displayed other pectin defective phenotypes, including reduced seed coat mucilage (47) (Fig. 4*D*). These phenotypic deviations from wild type were not due to a downregulation of *QUA1* and *QUA2* in the *nks1* mutant background (*SI Appendix*, Fig. S6*B*). In fact, the expression of the *QUA*s was increased in the *nks1* mutants, perhaps signifying an attempt to compensate for the loss of NKS1.

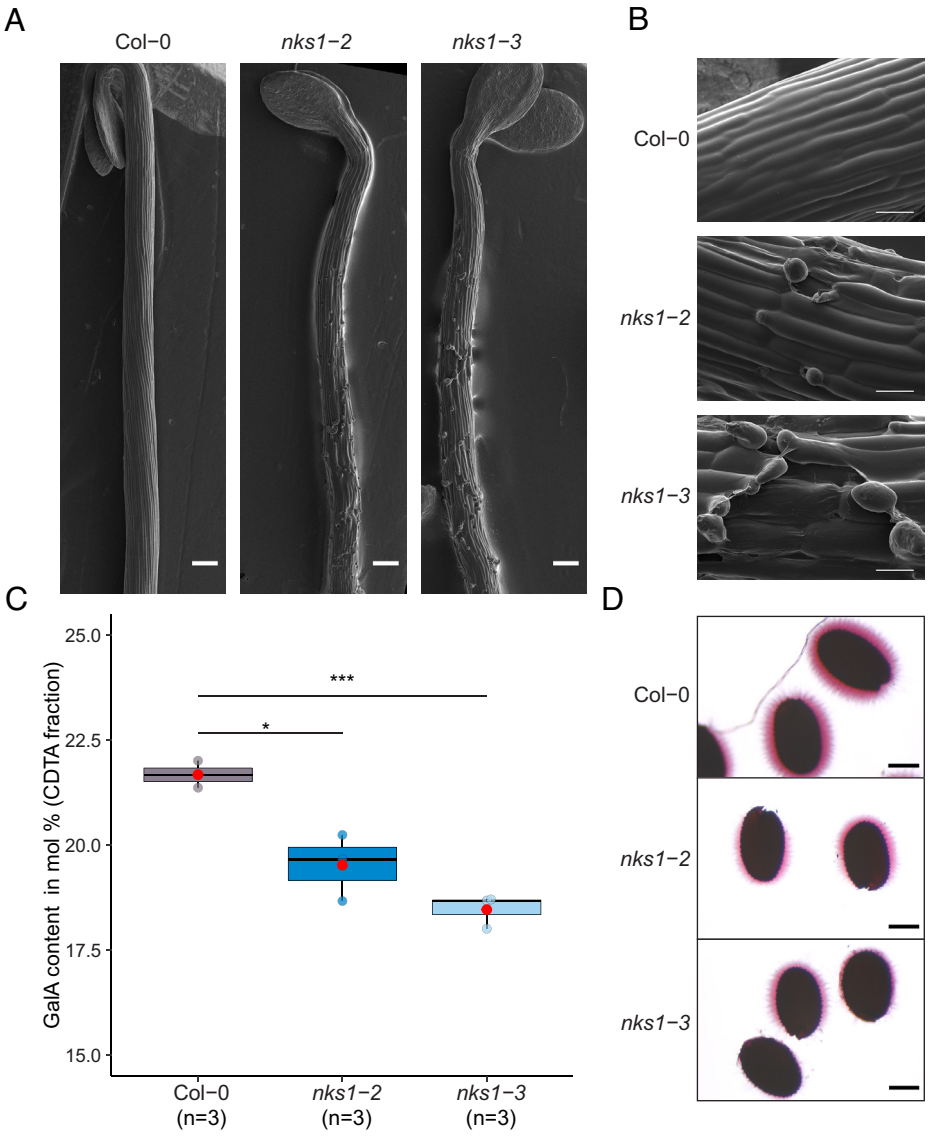

Fig. 4. *nks1* mutants are defective in cell adhesion and cell wall pectins. (*A*) Representative scanning electron microscopy images of 5-d-old etiolated seedlings of Col-0, *nks1-2,* and *nks1-3*. (*B*) Higher magnification of the seedlings shown in (*A*) showing epidermal cell layer in Col-0 and *nks1* alleles. (*C*) GalA levels in Col-0, *nks1-2,* and *nks1-3* in the CDTA-extracted cell wall fraction as measured by HPAEC-PAD. (*D*) Seed mucilage staining of Col-0, *nks1-2,* and *nks1-3* with Ruthenium Red solution. Asterisks in (*C*) indicate statistically significant difference between Col-0 and *nks1-3* as determined by unequal variance, two-tailed Student's *t* test, where ***$P < 0.0005$, *$P < 0.05$. Data are shown in boxplot where plot box limits indicate 25th and 75th percentiles, whiskers extend to 1.5 times the interquartile range, median is indicated by a horizontal line, mean by a red dot and individual data points are shown, and n (distinct pools of homogenized seedlings) is indicated in parentheses. [Scale bars, 200 μm in (*A*), 50 μm in (*B*), 200 μm in (*D*).]

Despite *NKS1* coexpression with primary wall *CESA* genes (Dataset S1), we did not observe any significant differences in cellulose content between *nks1-3* and wild-type seedlings (*SI Appendix*, Fig. S6*C*). Similarly, there were no significant changes in fluorescently tagged CESA dynamics in the plasma membrane (48) in *nks1-3* mutant hypocotyl cells, compred to wild type (*SI Appendix*, Fig. S6*D*).

***nks1* Mutants Phenocopy *qua1* and *qua2* Pectin Synthesis Mutants and NKS1 Forms a Stable Protein Complex with HG Synthesis Enzymes.** The cell wall pectin and cell adhesion defects of *nks1* mutants were reminiscent of *qua1* (6) and *qua2* mutants (7), and *NKS1* was tightly coexpressed with *QUA1* and *QUA3* (Dataset S1). QUA1 is similar to GT8 family GalATs and QUA2 is methyltransferase; both have been implicated in HG synthesis (6, 7, 19). We therefore investigated whether *nks1* mutants shared other physiological, molecular, and genetic phenotypes with *qua1* and *qua2* mutants.

Cell adhesion mutants, including *qua1* and *qua2*, display increased pectin-related cell wall integrity signaling (49), such as increased expression of *FAD-LINKED OXIDOREDUCTASE* (*FADLox*), a marker gene associated with pectin responses (50, 51). Similar to the *qua* mutants, *nks1-2* and *nks1-3* showed significant increases in *FADLox* expression compared to wild type (*SI Appendix*, Fig. S7*A*). The *nks1* mutants also displayed increased accumulation of anthocyanins when grown on high sucrose–containing growth media (*SI Appendix*, Fig. S7*B*), which was observed in both the *qua1* and *qua2* mutants (6, 49, 52, 53).

Recently, Verger et al. (11) documented the importance of epidermal continuity for mechano-perception. By modulating turgor (by changing the osmotic potential of the growth media) they could rescue cell-adhesion defects in *qua1* and *qua2* mutants, possibly through a tension-adhesion mechanism connected to cortical microtubules (11). To test whether we could also restore the cell adhesion defects in *nks1* mutants, we grew seedlings on media with reduced osmotic potential, i.e., on "hard" media [2.5% agar; (11)] compared to control (0.8% agar). Interestingly, cell elongation and cell adhesion defects were significantly restored when *nks1* seedlings were grown on the hard media (*SI Appendix*, Fig. S7*C*).

Mutations in *ESMD1*, which encodes a putative O-fucosyltransferase GT106 family protein, can suppress the *qua1* and *qua2* growth and cell adhesion phenotypes (49). Introducing *esmd1-1* into *nks1-3* also suppressed the hypocotyl elongation and cell adhesion phenotypes of *nks1-3* (Fig. 5 *A* and *B*), implying that loss of *NKS1*, *QUA1*, and *QUA2* all affect the same cell wall sensing and/or response pathway. To directly test this hypothesis, we generated double mutants between

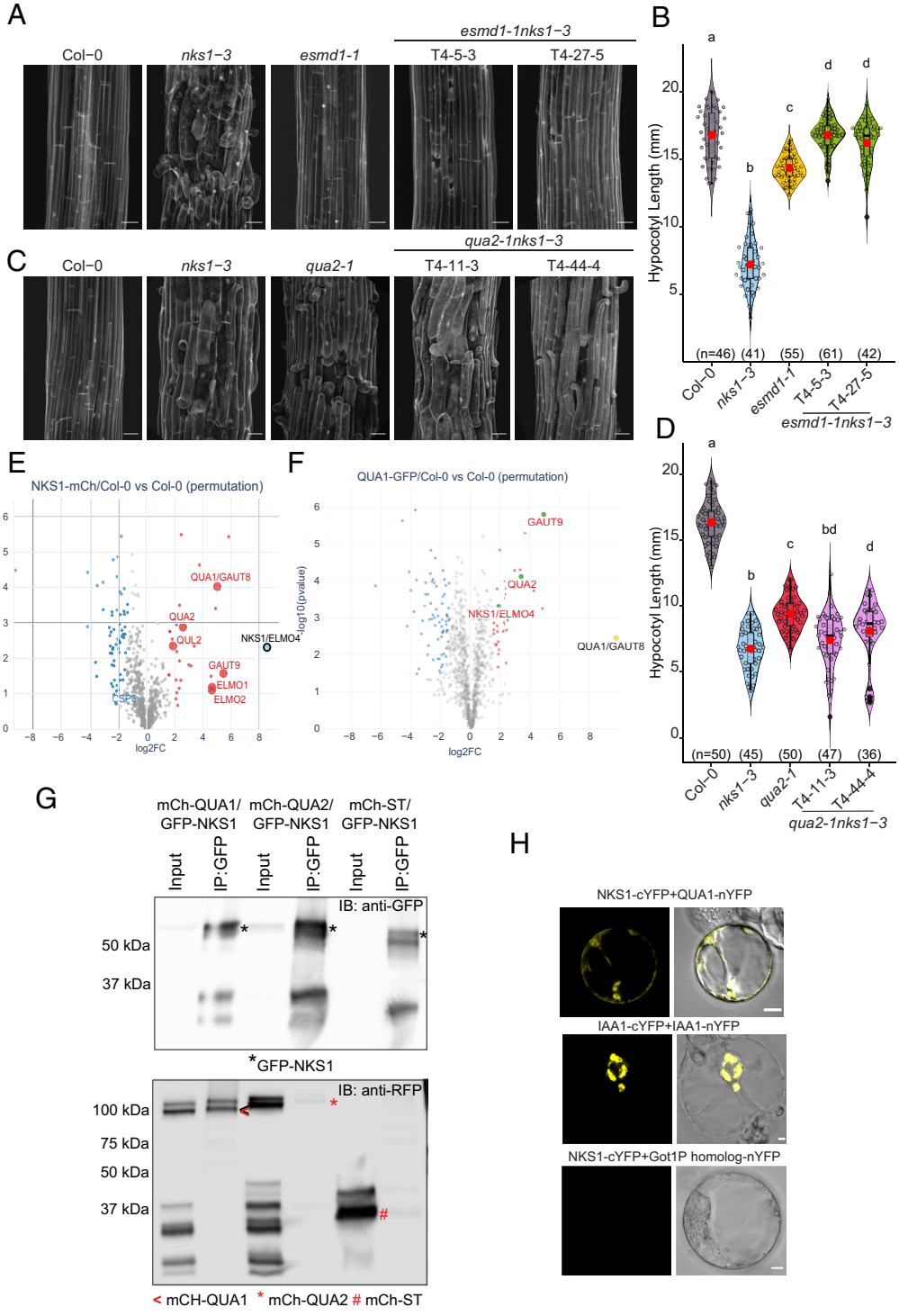

Fig. 5. NKS1 interacts with QUA1 and QUA2 and other pectin-synthesis-related proteins. (*A*) Representative z-projections (sum averages) of confocal stacks from propidium iodide-stained etiolated 5-d-old hypocotyl epidermal cell files from Col-0, *nks1-3*, *esmd1-1*, and two independent lines of *esmd1-1 nks1-3* double mutants. (*B*) Quantification of hypocotyl lengths of 6-d-old etiolated seedlings from Col-0, *nks1-3*, *esmd1-1*, and *esmd1-1 nks1-3* double mutants. (*C*) Representative z-projections (sum averages) of confocal stacks from propidium iodide-stained etiolated 5-d-old hypocotyl epidermal cell files from Col-0, *nks1-3*, *qua2-1*, and two independent lines of *qua2-1 nks1-3* double mutants. (*D*) Quantification of hypocotyl lengths of 6-d-old etiolated hypocotyls from Col-0, *nks1-3*, *qua2-1*, and *qua2-1 nks1-3* double mutants. (*E*) Volcano Plot showing significantly enriched or depleted (colored in red and dark blue, respectively) proteins from three independent NKS1–mRFP (light blue in plot) pulldown experiments in comparison to a WT control (N = three biological replicates per genotype). (*F*) Volcano Plot showing significantly enriched or depleted (colored in red and dark blue, respectively) proteins from three independent QUA1–GFP (yellow in plot) pulldown experiments in comparison to a WT control (N = three biological replicates per genotype. (*G*) Co-IP of mch-QUA1::GFP-NKS1, mch-QUA2::GFP-NKS1, and mch-ST::GFP-NKS1 transiently expressed in *N. benthamiana* leaves. Protein extracts were immunoprecipitated by anti-GFP beads, and interactions were detected by immunoblotting using anti-GFP and anti-RFP. mCh-QUA1 (97 kDa); mCh-QUA2 (110 kDa); GFP–NKS1 (53 kDa); mCh-NKS1 (52 kDa); mCh-ST (38 kDa); GFP-ST (40 kDa). (*H*) Representative images of bimolecular fluorescence complementation (BiFC) assay in *Arabidopsis* root cell culture protoplasts showing interaction between NKS1 (–cYFP) and QUA1 (GAUT8) (–nYFP). IAA1–cYFP and IAA1–nYFP was used as a positive control and NKS1 (–cYFP) and Got1P homolog (–nYFP) as negative control. Letters in (*B*) and (*D*) specify statistically significant differences among samples as determined by one-way ANOVA followed by Tukey's HSD test ($P < 0.05$). In violin plots, data distribution is outlined by the shape, plot box limits indicate 25th and 75th percentiles, whiskers extend to 1.5 times the interquartile range, median is indicated by a horizontal line, mean by a red dot and individual data points are shown, and n (seedlings) is indicated in parentheses. [Scale bars, 5 μm in (*A* and *C*); 10 μm in (*G*).]

nks1-3 and *qua2-1*. Because the *qua1-1* is in the Ws-4 background, we focused our efforts on the *qua2-1* which, like the *nks1* alleles, is in Col-0 background. We found that *nsk1-3 qua2-1* double mutants resembled the single mutants, which is consistent with the hypothesis that *NKS1* and *QUA2* act in the same complex or pathway (Fig. 5 *C* and *D*).

As the bulk of the NKS1 resides inside the Golgi lumen (*SI Appendix*, Fig. S3*D*), but the DUF1068 sequence does not harbor any hallmarks of enzymatic activity, we wondered whether NKS1 might physically interact with QUA1 and QUA2, forming a pectin biosynthesis protein complex. To test this hypothesis, we performed immunoprecipitation (IP) of NKS1–mRFP followed by LC–MS/MS analysis. We identified 27 proteins that were significantly enriched against the control with NKS1 being the top hit (Fig. 5*E* and Dataset S3). In addition, approximately 30 % of the 27 proteins were related to pectin synthesis. Importantly, QUA1 and QUA2 were identified among the top putative NKS1 interactors together with the NKS1 homologs ELMO1 and ELMO2, the QUA1 homolog GAUT9 and the QUA2-like protein QUL2. IP experiments using the Golgi-localized ST-mRFP, revealed no overlap with the NKS1–mRFP IP top hits. In addition, we generated a stable QUA1–GFP *Arabidopsis* line and performed IP experiments similar to those for NKS1–mRFP. Here, we found NKS1, QUA2, and GAUT9 as top hits (Fig. 5*F* and Dataset S3), confirming that these proteins form a pectin synthesis protein complex.

To corroborate that NKS1 interacts with QUA1 and QUA2, we performed co-IP experiments using heterologously expressed GFP–NKS1. We found strong interactions between GFP–NKS1 and mCherry-QUA1, but only weak interactions between GFP–NKS1 and mCherry–QUA2 (Fig. 5*G*). These data indicate a stronger interaction between NKS1 and QUA1 than with QUA2. This is in agreement with protein–protein docking simulations (cluster 1 with significant HADDOCK score of <−140; *SI Appendix*, Fig. S8*A*), which indicates possible interactions between NKS1 and QUA1 and between QUA1 and QUA2 (*SI Appendix*, Fig. S8*B*). These data were further confirmed by BiFC assays using *Arabidopsis* root cell suspension culture protoplasts. Here, we detected clear positive interactions between NKS1 and QUA1, which localized to small intracellular puncta resembling the Golgi apparatus, but we did not observe any signs of interaction between NKS1 and another Golgi localized protein, Got1p (Fig. 5*H*).

Taken together, our data imply that NKS1, QUA1, and QUA2 act together with several other pectin-related proteins to coordinate pectin synthesis in the Golgi.

Discussion

Domain of Unknown Function proteins are classified by sequence similarity to each other but not to any protein of known function and make up almost 22% of all proteins in the Pfam database (54). NKS1 belongs to the DUF1068 family, members of which are only found in land plants (Embryophyta), and almost all annotated DUF1068 proteins consist entirely of only the DUF1068 domain, making it difficult to deduce their function from protein sequence. Previous studies had implicated NKS1 in salt tolerance (30); we hypothesize that the high concentration of sucrose in the media used by Choi et al. (30) exacerbated the cell wall phenotype, since there are complex relationships between sugar availability and cell wall integrity responses (55, 56). NKS1 is part of a protein family referred to as ELMO (20, 21). ELMO1, which is distantly related to NKS1/ELMO4 (*SI Appendix*, Fig. S3), can also interact with QUA1 and NKS1 in heterologous systems (21), further supporting our results for NKS1/ELMO4. Here, we show that NKS1 maintains Golgi apparatus structure and function and is an integral part of a larger pectin synthesis protein complex.

Changes in pectin synthesis have been correlated with changes to Golgi structure (57, 58). For example, in seed coat epidermal cells, which synthesize an extraordinary volume of pectic mucilage during their development, Golgi stacks showed swollen margins, many associated vesicles, and a complex *trans*-Golgi network, while these changes were not observed in mutants lacking a key pectin synthesis gene (57). Whether these structural changes to the Golgi reflect an active remodeling of the endomembrane system or are a passive consequence of polysaccharide flux through the Golgi remains to be determined (26). Notably, in mammalian (HeLa) cells, changes to Golgi protein interactions were correlated with loss of GT function and dramatic changes to Golgi structure (59), implying an important relationship between Golgi structure and function. These data are consistent with our characterization of *nks1* mutants, in which both pectin synthesis and Golgi structure were defective. While the relationship between Golgi structure and function remains elusive, modeling has demonstrated that both changes to Golgi lipid composition and changes to curvature-generating proteins (i.e., vesicle trafficking machinery) can influence Golgi shape (60). According to this model, changes to pectin synthesis in *nks1* Golgi stacks might passively reshape the Golgi apparatus, perhaps due to changes in vesicle trafficking.

The seedling phenotypes of *nks1* mutants are strikingly similar to those of *qua1* and *qua2* mutants, including reduced cell elongation, cell adhesion defects, and suppression of the phenotypes under hyperosmotic conditions or by loss of ESMD (49). QUA1 is a predicted GalAT implicated in HG backbone synthesis (6), while QUA2 is an HG methyltransferase (7, 19). NKS1 lacks any sequence features that might suggest that it is directly involved in pectin synthesis. However, the interactions between NKS1 and QUA1 and QUA2 led us to hypothesize that NKS1 could play a role in organizing the pectin synthesis machinery in the Golgi apparatus by mediating close associations between QUA1 and QUA2. This scenario is in agreement with our protein–protein docking simulations of QUA1, QUA2, and NKS1. Notably, in this model, NKS1 is proposed to provide a supporting backbone structure for QUA1 that in turn may interact with QUA2 (*SI Appendix*, Fig. S8). These data support our co-IP studies, in which NKS1 bound strongly to QUA1 but less strongly to QUA2. In addition, ref. 21 found that ELMO1 can interact with QUA1, but not with QUA2, in yeast-interaction assays. Our IP analyses further indicate that the NKS1 is potentially part of a larger pectin synthesis protein complex, containing several pectin-related GTs and NKS1/ELMO homologs (including ELMO1).

Studies of HG synthesis have documented interactions between GAUT1 and GAUT7 (3), indicative of coordination among pectin synthesis proteins. While enzymatic activity has only been documented for GAUT1 (61), GAUT7 is required for proper GAUT1 localization to the Golgi (3), and GAUT7 can increase GAUT1 activity in vitro (62). HG is secreted in a highly methylesterified form, presumably to prevent it from forming calcium bridge-mediated aggregations before its incorporation into the cell wall. Quantitative immunolabeling of HG in pectin-synthesizing Golgi stacks predicted that HG methylesterification is highly efficient and nearly simultaneous with HG backbone synthesis, suggesting that the enzymes for pectin backbone formation and methylesterification act in concert (8). Indeed, *qua2* methyltransferase mutants do not display any changes to pectin methylesterification status but do show overall decreases in pectin synthesis (19). These results suggest that the HG that is synthesized in *qua2* mutants is efficiently methylesterified by other methyltransferases and that HG synthesis and methylesterification are tightly coupled. Therefore,

we propose a model in which NKS1/ELMO4, and other ELMO proteins, such as ELMO1 (21), mediate interactions between several HG-producing proteins, including the GalATs and putative GalATs, QUA1, GAUT9, and the HG methyltransferases, QUA2 and QUL2, thus providing a basis for these proteins to facilitate efficient and coordinated HG synthesis and methylesterification before pectin secretion.

Methods

For full methods, see *SI Appendix*.

Plant Material and Growth Conditions. *A. thaliana* ecotype Columbia (Col-0) and various transgenic lines *nks1-2* (SALK_151073), *nks1-3* (GK-228H05), *qua2-1*, *esmd1-1*, and fluorescent marker lines (*SI Appendix*, Table S3) were grown on square petri plates of half Murashige and Skoog (MS) nutrient mix (Duchefa), 0.5% sucrose and 0.8% (w/v) plant agar (Duchefa; pH 5.8). In some instances, seedlings were transferred to 6 cm and/or 10 cm-sized pots filled with soil.

The growth period of seedlings varied in different experiments as indicated in figure legends. Plants were genotyped using the primers indicated in *SI Appendix*, Table S4.

Brightfield Microscopy and Histology. Three- and six-day-old dark grown seedlings were scanned using an EPSON perfection V600 photo scanner and hypocotyl lengths and growth kinetics were measured (63). Seed mucilage was stained with 0.01% ruthenium red solution (11103-72-3, Sigma-Aldrich). The seeds were suspended in water and imaged using a compound microscope (64). Six-day-old etiolated seedlings were stained in an aqueous solution of 0.05 % (w/v) Toluidine blue and imaged using a compound microscope (65, 66).

In Silico Analyses.

NKS1 gene expression. *NKS1* (At4g30996) gene expression patterns were accessed via ePlant [https://bar.utoronto.ca/eplant/; (67)].

Coexpression analyses. Genes coexpressed with *NKS1* were identified using ATTED-II [https://atted.jp/; (28); Dataset S1].

Gene ontology (GO) analyses. GO analyses were conducted via the GO Resource interface (http://geneontology.org/; Dataset S2).

Protein domain structure prediction. Predicted protein domain architecture was accessed via InterPro [https://www.ebi.ac.uk/interpro/about/interpro/; (68)]. Transmembrane spanning helices were predicted using the TMHMM Server v.2.0 [https://www.cbs.dtu.dk/services/TMHMM/; (41)] or the newer DeepTMHMM version [https://dtu.biolib.com/DeepTMHMM; (69)].

Protein modeling and docking. Protein models were retrieved from the AlphaFold Protein Structure Database and trimmed for disordered regions and transmembrane domains. The HADDOCK 2.4 server was used for protein–protein docking with trimmed protein models and interface definitions as input (70, 71).

Phylogenetic analyses. NKS1 amino acid sequence was used to search homologs against publicly available database such as PLAZA (72), NCBI (https://www.ncbi.nlm.nih.gov/), and Phytozome (73). The identified protein sequences were used to construct phylogenetic tree according to ref. 74.

Gene Expression Analyses by qRT-PCR and RT-PCR. Total RNA was isolated from 6-d-old etiolated seedlings using RNeasy Plant minikit (74904, QIAGEN). cDNA was synthesized using iScript cDNA synthesis kit (Bio-Rad). *NKS1* transcript levels were analzsed by real time quantitative PCR (qRT-PCR). The relative expression values were calculated by the $2^{-\Delta\Delta Cq}$ method using Reference Gene Index (RGI). The relative expression of *FADLox*, *QUA1*, and *QUA2* was measured using CFX Touch Real-Time PCR detection system, Bio-Rad, and relative expression values were calculated by the $2^{-\Delta\Delta Cq}$ method using UBI10 (At4g05320) as a reference gene (*SI Appendix*, Table S4).

Semiquantitative RT-PCR was performed by intron spanning primers for *NKS1* and the *APT1* as control (*SI Appendix*, Table S4).

BiFC. *NKS1*, *QUA1*, *QUA2*, *Got1P* homolog (74), and *IAA1* (75) were PCR amplified from *Arabidopsis* Col-0 cDNA (*SI Appendix*, Table S4) and cloned into pDONR207 using BP Clonase Enzyme II. Entry clones were then subcloned into BiFC-specific destination vectors (pDEST-gwVYCE and pDEST-gwVYNE) (76) The clones were confirmed by PCR and restriction digestions followed by sequencing.

Protoplasts were isolated from *Arabidopsis* root suspension culture cells in enzyme solution and centrifuged, and pellets were washed. Protoplasts were resuspended and incubated with plasmids in 25% PEG 6000 solution, followed by addition of 500 μL 0.275 M $Ca(NO_3)_2$, centrifuged, resuspended, and incubated in dark for 16 h. Transfected protoplasts were documented using a Zeiss LSM880 confocal scanning microscope.

GO-PROMPTO Assay. GO-PROMTO assay (42) with VENUS as the fluorescent marker (77) was used to determine the topology of NKS1. The *NKS1* CDS was amplified (*SI Appendix*, Table S4) and cloned into pSUR, and transformed into *Agrobacterium tumefaciens*. Transient expression in *N. benthamiana* leaves and imaging was carried out as previously described in ref. 78.

Generation of NKS1–GFP/mRFP and QUA1–GFP Translational Fusion Constructs. The coding sequences of *NKS1* and *QUA1* with or without stop codon were amplified by PCR (*SI Appendix*, Table S4) from cDNA. The fragments were introduced into pENTR-D-TOPO vectors and cloned into plant expression vectors (79) by Gateway LR clonase mix (11791-019, Life Technologies). The resultant constructs were transformed into *Arabidopsis* by *A. tumefaciens* via floral dip (80).

Live-Cell Imaging and Analyses.

Low water potential treatment and imaging of cell–cell adhesion defect phenotype. Water potential of ½ MS growth media was changed as described in ref. 11. The seedlings were stained with propidium iodide and imaged using Zeiss LSM 780 or 880 confocal laser scanning microscope and images were analyzed using Fiji software.

Spinning disk microscopy. All other live cell imaging was conducted using CSU-X1 or CSU-W1 Yokogawa spinning disk head fitted to a Nikon Ti-E inverted microscope. For seedling imaging, 3-d-old etiolated hypocotyls or roots were mounted in water under an agarose pad. For BFA-treatments, seedlings were treated with BFA (50 μM) in ½ MS media with 1% sucrose. FM4-64 straining was performed for 10 min with 2 μM FM4-64.

Live cell image analyses. All image processing was performed using Fiji software. Colocalization between NKS1–GFP or NKS1–mRFP and compartment marker lines was analyzed as described by Gendre et al. (81), using the JaCOP plugin. Simultaneous dual-wavelength imaging was done by aligning two cameras relative to a calibration slide, then regions of interest were selected for colocalization analysis. Colocalization was quantified from z-stacks using the DiAna plugin for Fiji (82). CESA speed and density measurements were based on images with 10 s time intervals for 600 s and images were corrected for drift using StackReg. CESA speed and density were determined according to Sampathkumar et al. (83). Golgi movement was tracked using Fiji-TrackMate (84). The parameter "Mean Speed" was used to calculate the average Golgi motility rate. FM4-64 internalization was estimated from maximum fluorescence intensities of BFA bodies and compared to the plasma membrane intensities using Fiji (85). PIN2–GFP recycling was estimated in Fiji via the ratio of plasma membrane:intracellular signal. The number of BFA bodies was manually counted per unit area.

Cell Wall Analyses. Cell wall analyses were conducted on 6-d-old etiolated seedlings washed with 70% ethanol, dried, ground, and washed with 1:1 chloroform:methanol, then washed with acetone, and dried to obtain cell wall material (CWM). Then, 0.5 to 1 mg CWM was weighed in tubes and treated with trifluoroacetic acid. Samples were used for cellulose estimation by modified Seaman analysis by Anthrone assay (86, 87). Monosaccharides were analyzed from alcohol insoluble residue that was sequentially extracted into pectin and hemicellulose fractions using HPAEC as previously described (88).

Immunoprecipitation of NKS1–mRFP, QUA1–GFP, and Interactors. Leaves were homogenized, centrifuged, and mixed with 25 μL RFP-Trap Agarose or GFP-Trap Agarose (ChromoTek). Beads were spun down, washed, and stored at −80 until mass spectrometry analysis. The washed beads were incubated for 30 min with elution buffer. Tryptic peptide mixtures were loaded on Evotips (Evosep) and peptides were separated and injected via a CaptiveSpray source and 10-μm emitter into a timsTOF pro mass spectrometer (Bruker) ran in PASEF mode (89).

Raw mass spectrometry data were analyzed with MaxQuant against the *Arabidopsis* Uniprot FASTA database. Statistical analyses of LFQ-derived protein expression data were performed using the automated analysis pipeline of the Clinical Knowledge Graph (90). Differentially expressed proteins in each group

comparison were identified by SAMR multiclass test with permutation-based FDR correction for multiple hypothesis, followed by post hoc pairwise comparison unpaired *t* tests using the same parameters and permutation-based FDR correction (91). Significantly regulated proteins are colored in red and blue in the volcano plots for up and down-regulated proteins, respectively.

Western Blotting. Two-week-old seedlings were harvested, and total protein was quantified by the Bradford method. Proteins were separated by SDS-PAGE and detected by Western blot analysis (anti-GFP from rat [Chromotek, 3H9, 1:3,000], anti-RFP from Mouse [ChromoTek, 6G6, 1:2,000], anti-rat IgG produced in goat [Amersham, GE NA935, 1:10,000] and Anti-Mouse- in rabbit [Agilent, P0260, 1:10,000]).

Co-IP of Proteins From Transient Infiltration of Tobacco Leaves. *NKS1*, *QUA1*, *QUA2*, and transmembrane domain of rat ST were cloned into pDONR221. Entry clones were then subcloned into pFRET-gc-2in1-NN vectors (92) with fluorescent tags facing cytosol. Plasmids were transiently expressed in *N. benthamiana* leaves and Co-IP was performed according to ref. 93. (Co) immunoprecipitated proteins were separated on SDS-PAGE and detected by western blot analysis.

TEM and Transmission Electron Tomography (ET). For both TEM and tomography, etiolated 3-d-old seedlings were cryofixed using a Leica HPM-100 high-pressure freezer (94). Freeze-substitution was performed a Leica AFS2 automatic freeze substitution unit. Samples were then infiltrated with Spurr's Resin.
TEM. First, ~80-nm thick (silver) sections were cut and placed on mesh grids coated with 0.3% formvar. Grids were imaged with a Phillips CM120 BioTWIN TEM. Golgi features of genotype-blinded images were manually measured in Fiji.
ET. Five serial sections ~250 to 300 nm thick were cut were cut using a UC7 Ultramicrotome, placed on Maxtaform grids coated with 0.8% formvar and then coated with colloidal gold (Ted Pella) as a fiducial marker. Samples were imaged with a FEI Tecnai F30 TEM. Dual-axis tomograms were collected in a tilt range of +65° to −65° with 2° tilt steps per image. Tomograms were aligned, reconstructed, and modeled in Etomo and IMOD (95). Tomograms were manually segmented using IMOD.

Cryo-Scanning Electron Microscopy. Etiolated 3-d-old seedlings were processed according to ref. 96. Seedlings were mounted in Tissue-Tek on a sample holder, plunge-frozen, transferred to a cryostage and samples were coated with 60:40 gold–palladium alloy and then transferred into the FEI Quanta cryo scanning electron microscope.

Data, Materials, and Software Availability. Proteomics data have been deposited in identification of potential interactors of NKS1 and QUA1 (PXD047727) (97, 98).

ACKNOWLEDGMENTS. Some live cell imaging was conducted at Biological Optical Microscopy Platform (University of Melbourne) and electron microscopy at the Melbourne Advanced Microscopy Facility. We acknowledge the Proteomics Research Infrastructure at University of Copenhagen for the LC–MS/MS analyses. R.S.L. acknowledges PhD scholarship from Deutscher Akademischer Austausch Dienst [PKZ:91540412 (formerly A/10/75281)] at Max Planck Institute of Molecular Plant Physiology; Germany and postdoctoral grant from Kempe foundation (# SMK-1759) to R.P.B. at Umea Plant Science Center, Sweden. H.E.M. acknowledges an Australian Research Council Discovery Early Career Researcher Award (DE170100054), Canadian Natural Sciences and Engineering Research Council Discovery Grant (2020-05959) and funding from the Canada Research Chairs program as Canada Research Chair in Plant Cell Biology. C.K. and S.P. acknowledge funding from the Novo Nordisk Foundation (Emerging Investigator grant, NNF20OC0060564) and from the Lundbeck foundation (Experiment grant, R346-2020-1546). B.E. acknowledges ARC Future Fellowship and Discovery Project Awards (FT160100276 and DP180102630) and the Inaugural Fellowship from the University of Melbourne Botany Foundation. E.A.R.-R. is supported by a Consejo Nacional de Ciencia y Tecnología Beca de Posgrado en el Extranjero (2020-000000-01EXTF-00193). G.A.K. acknowledges an ARC Discovery Early Career Researcher Award (DE210101200) and a Swiss NSF Grant (P400PB_180834/1). N.N. acknowledges funding from Erasmus+ (NL GRONING03). S.P. acknowledges the financial aid of a Villum Investigator (Project ID: 25915), Danish National Research Foundation Chair (DNRF155), and Novo Nordisk Laureate (NNF19OC0056076) grants. K.F. acknowledges the Novo Nordisk Foundation for an Industrial Biotechnology and Environmental Biotechnology Postdoctoral grant (NNF21OC0071799) and the Villum Foundation for an Experiment grant (VIL50427).

Author affiliations: [a]Copenhagen Plant Science Center, Department of Plant & Environmental Sciences, University of Copenhagen, Frederiksberg C 1871, Denmark; [b]Max-Planck Institute for Molecular Plant Physiology, Potsdam 14476, Germany; [c]Umeå Plant Science Centre, Department of Forest Genetics and Plant Physiology, Swedish University of Agricultural Sciences, Umeå SE-90187, Sweden; [d]Department of Cell & Systems Biology, University of Toronto, Toronto, ON M5S 3G5, Canada; [e]School of Biosciences, University of Melbourne, Parkville, VIC 3010, Australia; [f]Department of Animal, Plant and Soil Sciences, School of Agriculture, Biomedicine and Environment, La Trobe University, Bundoora, VIC 3086, Australia; [g]Department of Biology and Biotechnology, Ruhr University Bochum, Bochum 44780, Germany; and [h]Joint International Research Laboratory of Metabolic & Developmental Sciences, State Key Laboratory of Hybrid Rice, University of Adelaide Joint Centre for Agriculture and Health, School of Life Sciences and Biotechnology, Shanghai Jiao Tong University, Shanghai 200240, China

1. C. T. Anderson, J. J. Kieber, Dynamic construction, perception, and remodeling of plant cell walls. *Annu. Rev. Plant Biol.* **71**, 39–69 (2020), 10.1146/annurev-arplant-081519-035846.
2. C. T. Anderson, 'We be jammin': An update on pectin biosynthesis, trafficking and dynamics. *J. Exp. Bot.* **67**, 495–502 (2016), 10.1093/jxb/erv501.
3. M. A. Atmodjo *et al.*, Galacturonosyltransferase (GAUT)1 and GAUT7 are the core of a plant cell wall pectin biosynthetic homogalacturonan:galacturonosyltransferase complex. *Proc. Natl. Acad. Sci. U.S.A.* **108**, 20225–20230 (2011).
4. H. Temple, S. Saez-Aguayo, F. C. Reyes, A. Orellana, The inside and outside: Topological issues in plant cell wall biosynthesis and the roles of nucleotide sugar transporters. *Glycobiology* **26**, 913–925 (2016), 10.1093/glycob/cww054.
5. C. Rautengarten *et al.*, The Golgi localized bifunctional UDP-rhamnose/UDP-galactose transporter family of *Arabidopsis*. *Proc. Natl. Acad. Sci. U.S.A.* **111**, 11563–11568 (2014), 10.1073/pnas.1406073111.
6. S. Bouton *et al.*, QUASIMODO1 encodes a putative membrane-bound glycosyltransferase required for normal pectin synthesis and cell adhesion in *Arabidopsis*. *Plant Cell* **14**, 2577–2590 (2002), 10.1105/tpc.004259.
7. G. Mouille *et al.*, Homogalacturonan synthesis in *Arabidopsis thaliana* requires a Golgi-localized protein with a putative methyltransferase domain. *Plant J.* **50**, 605–614 (2007), 10.1111/j.1365-313X.2007.03086.x.
8. G. F. Zhang, L. A. Staehelin, Functional compartmentation of the Golgi apparatus of plant cells: Immunocytochemical analysis of high-pressure frozen- and freeze-substituted sycamore maple suspension culture cells. *Plant Physiol.* **99**, 1070–1083 (1992), 10.1104/pp.99.3.1070.
9. A. Peaucelle *et al.*, Pectin-induced changes in cell wall mechanics underlie organ initiation in *Arabidopsis*. *Curr. Biol.* **21**, 1720–1726 (2011), 10.1016/j.cub.2011.08.057.
10. A. Peaucelle, R. Wightman, H. Höfte, The control of growth symmetry breaking in the *Arabidopsis* hypocotyl. *Curr. Biol.* **25**, 1746–1752 (2015), 10.1016/j.cub.2015.05.022.
11. S. Verger, Y. Long, A. Boudaoud, O. Hamant, A tension-adhesion feedback loop in plant epidermis. *eLife* **7**, e34460 (2018), 10.7554/eLife.34460.
12. A. J. Bidhendi, B. Altartouri, F. P. Gosselin, A. Geitmann, Mechanical stress initiates and sustains the morphogenesis of wavy leaf epidermal cells. *Cell Rep.* **28**, 1237–1250.e6 (2019), 10.1016/j.celrep.2019.07.006.
13. K. T. Haas, R. Wightman, E. M. Meyerowitz, A. Peaucelle, Pectin homogalacturonan nanofilament expansion drives morphogenesis in plant epidermal cells. *Science* **367**, 1003–1007 (2020), 10.1126/science.aaz5103.
14. S. Uluisik *et al.*, Genetic improvement of tomato by targeted control of fruit softening. *Nat. Biotechnol.* **34**, 950–952 (2016), 10.1038/nbt.3602.
15. S. Y. Rhee, E. Osborne, P. D. Poindexter, C. R. Somerville, Microspore separation in the quartet 3 mutants of *Arabidopsis* is impaired by a defect in a developmentally regulated polygalacturonase required for pollen mother cell wall degradation. *Plant Physiol.* **133**, 1170–1180 (2003), 10.1104/pp.103.028266.
16. M. Ogawa, P. Kay, S. Wilson, S. M. Swain, *ARABIDOPSIS* DEHISCENCE ZONE POLYGALACTURONASE1 (ADPG1), ADPG2, and QUARTET2 are Polygalacturonases required for cell separation during reproductive development in *Arabidopsis*. *Plant Cell* **21**, 216–233 (2009), 10.1105/tpc.108.063768.
17. M. W. Lewis, M. E. Leslie, S. J. Liljegren, Plant separation: 50 ways to leave your mother. *Curr. Opin. Plant Biol.* **9**, 59–65 (2006), 10.1016/j.pbi.2005.11.009.
18. W. G. Willats *et al.*, Modulation of the degree and pattern of methyl-esterification of pectic homogalacturonan in plant cell walls. Implications for pectin methyl esterase action, matrix properties, and cell adhesion. *J. Biol. Chem.* **276**, 19404–19413 (2001), 10.1074/jbc.M011242200.
19. J. Du *et al.*, Mutations in the pectin methyltransferase QUASIMODO2 influence cellulose biosynthesis and wall integrity in *Arabidopsis*. *Plant Cell* **32**, 3576–3597 (2020), 10.1105/tpc.20.00252.
20. B. D. Kohorn *et al.*, Mutation of an *Arabidopsis* Golgi membrane protein ELMO1 reduces cell adhesion. *Development* **148**, 199420 (2021), 10.1242/dev.199420.
21. B. D. Kohorn *et al.*, Golgi ELMO1 binds QUA1, QUA2, GAUT9, and ELMO4 and is required for pectin accumulation in *Arabidopsis*. *PLoS ONE* **18**, e0293961 (2023), 10.1371/journal.pone.0293961.
22. H. T. Parsons *et al.*, Separating Golgi proteins from cis to trans reveals underlying properties of cisternal localization. *Plant Cell* **31**, 2010–2034 (2019), 10.1105/tpc.19.00081.
23. J. Harholt *et al.*, ARAD proteins associated with pectic Arabinan biosynthesis form complexes when transiently overexpressed in planta. *Planta* **236**, 115–128 (2012), 10.1007/s00425-012-1592-3.
24. M. A. Atmodjo, Z. Hao, D. Mohnen, Evolving views of pectin biosynthesis. *Annu. Rev. Plant Biol.* **64**, 747–779 (2013), 10.1146/annurev-arplant-042811-105534.
25. O. A. Zabotina, N. Zang, R. Weerts, Polysaccharide biosynthesis: Glycosyltransferases and their complexes. *Front. Plant Sci.* **12**, 625307 (2021), 10.3389/fpls.2021.625307.
26. N. Hoffmann, S. King, A. L. Samuels, H. E. McFarlane, Subcellular coordination of plant cell wall synthesis. *Dev. Cell* **56**, 933–948 (2021), 10.1016/j.devcel.2021.03.004.
27. B. Usadel *et al.*, Co-expression tools for plant biology: Opportunities for hypothesis generation and caveats. *Plant Cell Environ.* **32**, 1633–1651 (2009), 10.1111/j.1365-3040.2009.02040.x.

28. T. Obayashi, Y. Aoki, S. Tadaka, Y. Kagaya, K. Kinoshita, ATTED-II in 2018: A plant coexpression database based on investigation of the statistical property of the mutual rank index. *Plant Cell Physiol.* **59**, e3 (2018), 10.1093/pcp/pcx191.
29. H. Temple *et al.*, Golgi-localized putative S-adenosyl methionine transporters required for plant cell wall polysaccharide methylation. *Nat. Plants* **8**, 656–669 (2022), https://www.nature.com/articles/s41477-022-01156-4.
30. W. Choi *et al.*, NKS1, Na(+)- and K(+)-sensitive 1, regulates ion homeostasis in an SOS-independent pathway in *Arabidopsis*. *Phytochemistry* **72**, 330–336 (2011), 10.1016/j.phytochem.2010.12.005.
31. H. Batoko, H. Q. Zheng, C. Hawes, I. Moore, A rab1 GTPase is required for transport between the endoplasmic reticulum and golgi apparatus and for normal golgi movement in plants. *Plant Cell* **12**, 2201–2218 (2000), 10.1105/tpc.12.11.2201.
32. N. Geldner *et al.*, Rapid, combinatorial analysis of membrane compartments in intact plants with a multicolor marker set. *Plant J.* **59**, 169–178 (2009), 10.1111/j.1365-313X.2009.03851.x.
33. J. Dettmer, A. Hong-Hermesdorf, Y. D. Stierhof, K. Schumacher, Vacuolar H^+-ATPase activity is required for endocytic and secretory trafficking in *Arabidopsis*. *Plant Cell* **18**, 715–730 (2006), 10.1105/tpc.105.037978.
34. N. Geldner *et al.*, The *Arabidopsis* GNOM ARF GEF mediates endosomal recycling, auxin transport, and auxin-dependent plant growth. *Cell* **112**, 219–230 (2003), 10.1016/s0092-8674(03)00003-5.
35. M. Grebe *et al.*, *Arabidopsis* sterol endocytosis involves actin-mediated trafficking via ARA6-positive early endosomes. *Curr. Biol.* **13**, 1378–1387 (2003), 10.1016/s0960-9822(03)00538-4.
36. D. Gendre *et al.*, Conserved *Arabidopsis* ECHIDNA protein mediates trans-Golgi-network trafficking and cell elongation. *Proc. Natl. Acad. Sci. U.S.A.* **108**, 8048–8053 (2011), 10.1073/pnas.1018371108.
37. C. Saint-Jore-Dupas *et al.*, Plant N-glycan processing enzymes employ different targeting mechanisms for their spatial arrangement along the secretory pathway. *Plant Cell* **18**, 3182–3200 (2006), 10.1105/tpc.105.036400.
38. N. Nikolovski *et al.*, Putative glycosyltransferases and other plant Golgi apparatus proteins are revealed by LOPIT proteomics. *Plant Physiol.* **160**, 1037–1051 (2012), 10.1104/pp.112.204263.
39. H. T. Parsons *et al.*, Isolation and proteomic characterization of the *Arabidopsis* Golgi defines functional and novel components involved in plant cell wall biosynthesis. *Plant Physiol.* **159**, 12–26 (2012), 10.1104/pp.111.193151.
40. L. Renna *et al.*, Identification and characterization of AtCASP, a plant transmembrane Golgi matrix protein. *Plant Mol. Biol.* **58**, 109–122 (2005), 10.1007/s11103-005-4618-4.
41. A. Krogh, B. Larsson, G. von Heijne, E. L. Sonnhammer, Predicting transmembrane protein topology with a hidden Markov model: Application to complete genomes. *J. Mol. Biol.* **305**, 567–580 (2001), 10.1006/jmbi.2000.4315.
42. C. Søgaard *et al.*, GO-PROMTO illuminates protein membrane topologies of glycan biosynthetic enzymes in the Golgi apparatus of living tissues. *PLoS ONE* **7**, e31324 (2012), 10.1371/journal.pone.0031324.
43. M. Samalova, M. Fricker, I. Moore, Ratiometric fluorescence-imaging assays of plant membrane traffic using polyproteins. *Traffic* **7**, 1701–1723 (2006), 10.1111/j.1600-0854.2006.00502.x.
44. J. Xu, B. Scheres, Dissection of *Arabidopsis* ADP-RIBOSYLATION FACTOR 1 function in epidermal cell polarity. *Plant Cell* **17**, 525–536 (2005), 10.1105/tpc.104.028449.
45. C. Viotti *et al.*, Endocytic and secretory traffic in *Arabidopsis* merge in the trans-Golgi network/early endosome, an independent and highly dynamic organelle. *Plant Cell* **22**, 1344–1357 (2010), 10.1105/tpc.109.072637.
46. S. Bolte *et al.*, FM-dyes as experimental probes for dissecting vesicle trafficking in living plant cells. *J. Microsc.* **214**, 159–173 (2004), 10.1111/j.0022-2720.2004.01348.x.
47. T. L. Western, D. J. Skinner, G. W. Haughn, Differentiation of mucilage secretory cells of the *Arabidopsis* seed coat. *Plant Physiol.* **122**, 345–356 (2000), 10.1104/pp.122.2.345.
48. A. R. Paredez, C. R. Somerville, D. W. Ehrhardt, Visualization of cellulose synthase demonstrates functional association with microtubules. *Science* **312**, 1491–1495 (2006), 10.1126/science.1126551.
49. S. Verger, S. Chabout, E. Gineau, G. Mouille, Cell adhesion in plants is under the control of putative O-fucosyltransferases. *Development* **143**, 2536–2540 (2016), 10.1242/dev.132308.
50. C. Denoux *et al.*, Activation of defense response pathways by OGs and Flg22 elicitors in *Arabidopsis* seedlings. *Mol. Plant* **1**, 423–445 (2008), 10.1093/mp/ssn019.
51. B. D. Kohorn, S. L. Kohorn, N. J. Saba, V. M. Martinez, Requirement for pectin methyl esterase and preference for fragmented over native pectins for wall-associated kinase-activated, EDS1/PAD4-dependent stress response in *Arabidopsis*. *J. Biol. Chem.* **289**, 18978–18986 (2014), 10.1074/jbc.M114.567545.
52. P. Gao, Z. Xin, Z. L. Zheng, The OSU1/QUA2/TSD2-encoded putative methyltransferase is a critical modulator of carbon and nitrogen nutrient balance response in *Arabidopsis*. *PLoS ONE* **3**, e1387 (2008), 10.1371/journal.pone.0001387.
53. E. Krupková, P. Immerzeel, M. Pauly, T. Schmülling, The TUMOROUS SHOOT DEVELOPMENT2 gene of *Arabidopsis* encoding a putative methyltransferase is required for cell adhesion and co-ordinated plant development. *Plant J.* **50**, 735–750 (2007), 10.1111/j.1365-313X.2007.03123.x.
54. S. El-Gebali *et al.*, The Pfam protein families database in 2019. *Nucl. Acids Res.* **47**, D427–D432 (2019), 10.1093/nar/gky995.
55. T. Hamann, M. Bennett, J. Mansfield, C. Somerville, Identification of cell-wall stress as a hexose-dependent and osmosensitive regulator of plant responses. *Plant J.* **57**, 1015–1026 (2009), 10.1111/j.1365-313X.2008.03744.x.
56. T. Engelsdorf *et al.*, The plant cell wall integrity maintenance and immune signaling systems cooperate to control stress responses in *Arabidopsis thaliana*. *Sci. Signal* **11**, eaao3070 (2018), 10.1126/scisignal.aao3070.
57. R. E. Young *et al.*, Analysis of the Golgi apparatus in *Arabidopsis* seed coat cells during polarized secretion of pectin-rich mucilage. *Plant Cell* **20**, 1623–1638 (2008), 10.1105/tpc.108.058842.
58. P. Wang, X. Chen, C. Goldbeck, E. Chung, B. H. Kang, A distinct class of vesicles derived from the trans-Golgi mediates secretion of xylogalacturonan in the root border cell. *Plant J.* **92**, 596–610 (2017), 10.1111/tpj.13704.
59. J. Van Galen *et al.*, Sphingomyelin homeostasis is required to form functional enzymatic domains at the trans-Golgi network. *J. Cell Biol.* **206**, 609–618 (2014), 10.1083/jcb.201405009.
60. F. Campelo *et al.*, Sphingomyelin metabolism controls the shape and function of the Golgi cisternae. *eLife* **6**, e24603 (2017), 10.7554/eLife.24603.
61. J. D. Sterling *et al.*, Functional identification of an *Arabidopsis* pectin biosynthetic homogalacturonan galacturonosyltransferase. *Proc. Natl. Acad. Sci. U.S.A.* **103**, 5236–5241 (2006), 10.1073/pnas.0600120103.
62. R. A. Amos *et al.*, A two-phase model for the non-processive biosynthesis of homogalacturonan polysaccharides by the GAUT1:GAUT7 complex. *J. Biol. Chem.* **293**, 19047–19063 (2018), 10.1074/jbc.RA118.004463.
63. K. Jonsson *et al.*, Mechanochemical feedback mediates tissue bending required for seedling emergence. *Curr. Biol.* **31**, 1154–1164.e3 (2021).
64. H. E. McFarlane, D. Gendre, T. L. Western, Seed coat ruthenium red staining assay. *Bio-Protocols* **4**, e1096 (2014), 10.21769/BioProtoc.1096.
65. T. Tanaka, H. Tanaka, C. Machida, M. Watanabe, Y. Machida, A new method for rapid visualization of defects in leaf cuticle reveals five intrinsic patterns of surface defects in *Arabidopsis*. *Plant J.* **37**, 139–146 (2004), 10.1046/j.1365-313x.2003.01946.x.
66. L. Neumetzler *et al.*, The FRIABLE1 gene product affects cell adhesion in *Arabidopsis*. *PLoS ONE* **7**, e42914 (2012), 10.1371/journal.pone.0042914.
67. J. Waese *et al.*, ePlant: Visualizing and exploring multiple levels of data for hypothesis generation in plant biology. *Plant Cell* **29**, 1806–1821 (2017), 10.1105/tpc.17.00073.
68. M. Blum *et al.*, The InterPro protein families and domains database: 20 years on. *Nucl. Acids Res.* **49**, D344–D354 (2021), 10.1093/nar/gkaa977.
69. J. Hallgren *et al.*, DeepTMHMM predicts alpha and beta transmembrane proteins using deep neural networks. bioRxiv [Preprint] (2022), https://doi.org/10.1101/2022.04.08.487609 (Accessed 10 April 2022).
70. R. V. Honorato *et al.*, Structural biology in the clouds: The WeNMR-EOSC ecosystem. *Front. Mol. Biosci.* **8**, 729513 (2021).
71. G. C. P. Van Zundert *et al.*, The HADDOCK2.2 webserver: User-friendly integrative modeling of biomolecular complexes. *J. Mol. Biol.* **428**, 720–725 (2016), 10.1016/j.jmb.2015.09.014.
72. M. Van Bel *et al.*, PLAZA 4.0: An integrative resource for functional, evolutionary and comparative plant genomics. *Nucl. Acids Res.* **46**, D1190–D1196 (2018), 10.1093/nar/gkx1002.
73. D. M. Goodstein *et al.*, Phytozome: A comparative platform for green plant genomics. *Nucl. Acids Res.* **40**, D1178–D1186 (2012), 10.1093/nar/gkr944.
74. Y. Zhang *et al.*, Golgi-localized STELLO proteins regulate the assembly and trafficking of cellulose synthase complexes in *Arabidopsis*. *Nat. Commun.* **7**, 11656 (2016), 10.1038/ncomms11656.
75. S. K. Pandey *et al.*, LBD18 uses a dual mode of a positive feedback loop to regulate ARF expression and transcriptional activity in *Arabidopsis*. *Plant J.* **95**, 233–251 (2018), 10.1111/tpj.13945.
76. C. Gehl, R. Waadt, J. Kudla, R. R. Mendel, R. Hänsch, New GATEWAY vectors for high throughput analyses of protein protein interactions by bimolecular fluorescence complementation. *Mol. Plant* **2**, 1051–1058 (2009), 10.1093/mp/ssp040.
77. E. R. Lampugnani *et al.*, A glycosyltransferase from *Nicotiana alata* pollen mediates synthesis of a linear (1,5)-α-L-Arabinan when expressed in *Arabidopsis*. *Plant Physiol.* **170**, 1962–1974 (2016), 10.1104/pp.15.02005.
78. C. Sánchez-Rodríguez *et al.*, The cellulose synthases are cargo of the TPLATE adaptor complex. *Mol. Plant.* **11**, 346–349 (2018), 10.1016/j.molp.2017.11.012.
79. C. Grefen *et al.*, A ubiquitin-10 promoter-based vector set for fluorescent protein tagging facilitates temporal stability and native protein distribution in transient and stable expression studies. *Plant J.* **64**, 355–365 (2010), 10.1111/j.1365-313X.2010.04322.x.
80. S. J. Clough, A. F. Bent, Floral dip: A simplified method for Agrobacterium-mediated transformation of *Arabidopsis thaliana*. *Plant J.* **16**, 735–743 (1998), 10.1046/j.1365-313x.1998.00343.x.
81. D. Gendre *et al.*, Trans-Golgi network localized ECHIDNA/Ypt interacting protein complex is required for the secretion of cell wall polysaccharides in *Arabidopsis*. *Plant Cell* **25**, 2633–2646 (2013), 10.1105/tpc.
82. J. F. Gilles, M. Dos Santos, T. Boudier, S. Bolte, N. Heck, DiAna, an ImageJ tool for object-based 3D co-localization and distance analysis. *Methods* **115**, 55–64 (2017), 10.1016/j.ymeth.2016.11.016.
83. A. Sampathkumar *et al.*, Patterning and lifetime of plasma membrane–localized cellulose synthase is dependent on actin organization in *Arabidopsis* interphase cells. *Plant Physiol.* **162**, 675–688 (2013), 10.1104/pp.113.215277.
84. J. Y. Tinevez *et al.*, TrackMate: An open and extensible platform for single-particle tracking. *Methods* **115**, 80–90 (2017), 10.1016/j.ymeth.2016.09.016.
85. A. Gadeyne *et al.*, The TPLATE adaptor complex drives clathrin-mediated endocytosis in plants. *Cell* **156**, 691–704 (2014), 10.1016/j.cell.2014.01.039.
86. R. R. Selvendran, M. A. O'Neill, Isolation and analysis of cell walls from plant material. *Methods Biochem. Anal.* **32**, 25–153 (1987), 10.1002/9780470110539.ch2.
87. D. M. Updegraff, Semimicro determination of cellulose in biological materials. *Anal Biochem.* **32**, 420–424 (1969), 10.1016/s0003-2697(69)80009-6.
88. C. Rautengarten, J. L. Heazlewood, B. Ebert, Profiling cell wall monosaccharides and nucleotide-sugars from plants. *Bio-Protocols* **4**, e20092 (2019), 10.1002/cppb.20092.
89. F. Meier *et al.*, Online parallel accumulation–serial fragmentation (PASEF) with a novel trapped ion mobility mass spectrometer. *Mol. Cell Proteomics* **17**, 2534–2545 (2018), 10.1074/mcp.
90. A. Santos *et al.*, Clinical knowledge graph integrates proteomics data into clinical decision-making. biorxiv [Preprint] (2020), https://doi.org/10.1101/2020.05.09.084897 (Accessed 10 May 20220).
91. R. Tibshirani *et al.*, SAM: Significance analysis of microarrays. R package version 3 (2018). https://cran.r-project.org/web/packages/samr/index.html. Accessed 16 October 2018.
92. A. Hecker *et al.*, Binary 2in1 vectors improve in planta (co)localization and dynamic protein interaction studies. *Plant Physiol.* **168**, 776–787 (2015), 10.1104/pp.15.00533.
93. L. Y. Asseck *et al.*, Endoplasmic reticulum membrane receptors of the GET pathway are conserved throughout eukaryotes. *Proc. Natl. Acad. Sci. U.S.A.* **118**, e2017636118 (2021), 10.1073/pnas.2017636118.
94. H. E. McFarlane, R. E. Young, G. O. Wasteneys, A. L. Samuels, Cortical microtubules mark the mucilage secretion domain of the plasma membrane in *Arabidopsis* seed coat cells. *Planta* **227**, 1363–1375 (2008), 10.1007/s00425-008-0708-2.
95. J. R. Kremer, D. N. Mastronarde, J. R. McIntosh, Computer visualization of three-dimensional image data using IMOD. *J. Struct. Biol.* **116**, 71–76 (1996), 10.1006/jsbi.1996.0013.
96. H. E. McFarlane *et al.*, A G protein-coupled receptor-like module regulates cellulose synthase secretion from the endomembrane system in *Arabidopsis*. *Dev. Cell* **56**, 1484–1497 (2021), 10.1016/j.devcel.2021.03.031.
97. Y. Perez-Riverol *et al.*, The PRIDE database resources in 2022: a hub for mass spectrometry-based proteomics evidences. *Nucleic Acids Res.* **50**, D543–D552 (2022).
98. C. Kesten, L. Wang, S. Persson, Identification of potential interactors of NKS1 and QUA1. PRIDE: PRoteomics IDEntifications database. https://www.ebi.ac.uk/pride/archive/projects/PXD047727. Accessed 20 March 2024.